Supplementary Information for:

A Comparison of the Chemical, Optical and Electrocatalytic Properties of Water-Oxidation Catalysts for Use in Integrated Solar-Fuels Generators

Ke Sun[1], Ivan A. Moreno-Hernandez[1], William C. Schmidt, Jr.[1], Xinghao Zhou[2], J. Chance Crompton[1], Rui Liu[3], Fadl H. Saadi[2], Yikai Chen[3], Kimberly M. Papadantonakis[1], Nathan S. Lewis[1,4,5*]

[1] Division of Chemistry and Chemical Engineering,

[2] Department of Applied Physics and Materials Science,

[3] Joint Center for Artificial Photosynthesis,

[4] Beckman Institute and Molecular Materials Research Center,

[5] Kavli Nanoscience Institute,

California Institute of Technology, Pasadena, CA 91125, USA

*Corresponding author: nslewis@caltech.edu

I. EXPERIMENTAL DETAILS

A. Solvents and Prepared Solutions

All materials were used as received, except where otherwise noted. H_2O with a resistivity of 18.2 MΩ-cm was obtained from a Barnsted Nanopure system. 1.0 M KOH(aq) was prepared using potassium hydroxide pellets (Macron Chemicals, ACS 88%). A 1.0 M potassium borate solution (K-Bi) was prepared using a 1.0 M KOH(aq) solution made from potassium hydroxide pellets and 2.0 M aqueous boric acid (H_3BO_3, Sigma-Aldrich, BioReagent ≥99.5%). 1.0 M

H_2SO_4(aq) was prepared from sulfuric acid (J. T. Baker, ACS reagent, 95%-98%). 0.10 M potassium phosphate buffer (K-Pi) was prepared using a mixture of 0.10 M monobasic potassium phosphate (HK_2PO_4, Fisher Scientific, ACS >99%) and 0.10 M dibasic potassium phosphate solution (H_2KPO_4, Fisher Scientific, ACS >99%) with a volume ratio of 61.5: 38.5.

B. Catalyst Deposition and Electrode Preparation

1. Substrates

Glass slides coated with fluorine-doped tin oxide (FTO, TEC-15, Hartford) were soaked for 1 min in 1.0 M H_2SO_4(aq), thoroughly rinsed with H_2O, and then sequentially sonicated in acetone (CH_3COCH_3, EMD Millpore Corporation, ACS grade, 99.5%) and isopropanol (Wards Science, lab grade, ≥99%) for 5 min each. The FTO-coated glass substrates were rinsed with H_2O following each sonication step. The FTO-glass substrates were then dried under a stream of N_2(g) and diced into pieces having an approximate size of 1×1 cm.

2. Sputtered thin films

Thin films of Pt and Ni-Mo were deposited from Pt (Alfa, 99.99%) and Ni-Mo (Alfa, 99.99%) targets, respectively, onto FTO-glass substrates using a DC magnetron sputtering system (AJA International Inc.) at a chamber pressure of 5 mTorr and under a 20 sccm flow of Ar. The deposition power was 100 W for Pt and 150 W for Ni-Mo, respectively, and no stage heating was used. Pt deposition times of 23 sec, 1 min, and 13 min, respectively produced film thicknesses of 2 nm, 5 nm and 60 nm, respectively. The deposition times for Ni_xMo_y were 1 min (~2 nm), 5 min (~10 nm) and 10 min (~20 nm).

Thin films of NiO_x and IrO_x were deposited from Ni (Kurt Lesker, 2" diameter × 0.125" thickness, 99.95%) or Ir (99.9% from ACI Alloys, Inc.) targets onto FTO-glass substrates via

reactive RF sputtering using a high-vacuum magnetron sputtering system (AJA International Inc.). The maximum base pressure was 8×10^{-8} Torr, and the working pressure was held at 5 mTorr under a 20 sccm flow of Ar. For NiO_x films, the deposition rate was maintained at 0.2 Å s^{-1} by adjusting the sputtering power on the Ni target. The NiO_x films were 7 nm, 35 nm, and 70 nm thick, respectively, as measured by a calibrated stylus profilometer (DektakXT). The IrO_x catalyst layer was sputtered onto the FTO-coated glass substrates from an RF source at 200 W at 300 °C under a constant flow of 3.0/3.0 sccm Ar/O_2, while maintaining an overall pressure of 5 mTorr. Control of the deposition time yielded IrO_x film thicknesses of 10 nm (2 min), ~60 nm (10 min) and >100 nm (30 min), respectively.

3. Preparation of Electrodes

Silver paste (SPI supplies) was used to attach a Cu wire to the front side of each of the FTO-coated glass substrates. The Ag paste was allowed to dry in air for at least 1 h and then the Cu wire was threaded through a glass tube. The substrate was attached and sealed to the end of the glass tube using gray epoxy. All of the substrates were centered on the glass tubing and were oriented in a side-facing manner. The epoxy was allowed to cure in air for > 12 h. The exposed area of each electrode, as defined by the edge of the applied epoxy, was imaged with a high-resolution optical scanner and measured using ImageJ software. Exposed areas for the FTO-coated glass substrates were 0.3–0.4 cm^2, unless specified otherwise.

4. Electrodeposition of Thin Films

CoO_x films, $CoO_{x,ed}$, were deposited anodically onto FTO-coated glass electrodes followed by performing a pretreatment consisting of 10 voltammetric cycles in 1.0 M KOH(aq) at potentials between 0.0 and 0.8 V vs a Hg/HgO/1.0 M KOH(aq) reference electrode (CH

Instruments 152). The FTO-glass electrodes were then immersed in an aqueous solution that contained 10 mM cobalt nitrate hexahydrate ($Co(NO_3)_2 \cdot 6H_2O$ Alfa Aesar, ACS grade, ≥98%) and 0.10 M sodium acetate anhydrate ($NaOOCCH_3$ Sigma Aldrich, >99%).[1] The pH of the solution was 7.5. The deposition was conducted using a three-electrode configuration with a fritted Pt mesh (Aldrich) counter electrode and a saturated calomel electrode, SCE (CH Instruments 150), as a reference electrode. The current density was maintained at 76 μA cm^{-2}, and no bubbles were observed during deposition. The deposition was performed until the total charge density passed was between 5 mC cm^{-2} and 120 mC cm^{-2}, which required 1–25 min, depending on the desired film thickness.

Cobalt phosphate films, Co-Pi, were deposited anodically onto FTO-glass electrodes from a fresh aqueous precursor solution that consisted of 0.10 M potassium phosphate, K-Pi, and 0.50 mM cobalt nitrate ($Co(NO_3)_2$ Alfa Aesar, ACS grade, ≥98%).[2] The K-Pi solution was prepared by mixing an aqueous 0.10 M solution of dibasic potassium phosphate (H_2KPO_4, Fisher Scientific, ACS >99%) with an aqueous 0.10 M solution of monobasic potassium phosphate (HK_2PO_4, Fisher Scientific, ACS >99%) such that the K-Pi solution was 0.062 M K_2HPO_4 and 0.038 M KH_2PO_4. Electrodeposition was performed at room temperature under galvanostatic control in a two-compartment cell, with a current density of 0.10 mA cm^{-2}. The solution was neither stirred nor agitated during the deposition. A fritted Pt mesh served as the counter electrode and a SCE (calibrated to 0.654 V versus a reversible hydrogen electrode, RHE) served as the reference electrode. The deposition was continued until 5–120 mC cm^{-2} had been passed, depending on the desired thickness for the film. Samples were then rinsed with H_2O and dried under a stream of $N_2(g)$.

$Ni(OH)_2$ and $Ni_xFe_{1-x}(OH)_y$ films were electrodeposited cathodically onto FTO-glass electrodes. Prior to deposition, the substrates were immersed in 1.0 M KOH(aq) and cycled ten times through the potential range of 0.0 to 0.8 V versus a Hg/HgO reference electrode (CH Instruments) with a fritted Pt mesh counter electrode. Films of $Ni(OH)_2$ were deposited from an unstirred aqueous solution of 0.10 M $Ni(NO_3)_2 \cdot 6H_2O$ (Sigma Aldrich, 99.999% trace-metals basis). Films of $Ni_xFe_{1-x}(OH)_y$ were deposited from unstirred solutions with a total metal content of 0.10 M, with Fe accounting for 25% of the metal content, 5 mM $Ni(NO_3)_2 \cdot 6H_2O$ (Sigma Aldrich, 99.999% trace-metals basis) and 5 mM $FeSO_4 \cdot 7H_2O$ (Sigma Aldrich, ACS reagent, ≥99.0%). To prevent precipitation, the Ni solution was purged with Ar(g) for at least 30 s prior to addition of the Fe salt. Depositions were conducted for 2-10 s using a current density of −10 mA cm^{-2}, resulting in nominal film thicknesses of 7-40 nm.

5. Atomic-layer Deposition

CoO_x films, $CoO_{x,ALD}$, were deposited onto FTO-glass substrates via atomic-layer deposition (ALD) using a Cambridge Nanotech S200 ALD system. The cobaltocene (bis(cyclopentadienyl)cobalt(II), Cp_2Co, Strem, 98%) precursor was heated to 80 °C and maintained at that temperature during the deposition, which was conducted using a substrate temperature of 150 °C. Each ALD cycle consisted of a 2 s pulse of the cobaltocene precursor, a 10 s purge under a 20 cm^3 min^{-1} flow of research-grade N_2(g), a 5 s ozone pulse, and a further 10 s N_2(g) purge. 60-1000 ALD cycles were performed to produce film thicknesses of 2-50 nm.

C. Scanning Electron Microscopy

Images of electrocatalyst films were collected using a calibrated Nova NanoSEM 450 (FEI) SEM with an accelerating voltage of 5 kV.

D. Electrochemical Measurements

A three-necked flask was used for all electrochemical measurements. Cyclic voltammetry, current interruption for resistance correction, and in situ electrochromism data were obtained using a Biologic MPG-2-44 potentiostat (Bio-Logic Science Instruments). The cyclic voltammetric data were recorded at a scan rate of 10 mV s^{-1}. Current interruption at a current density of 10 mA cm^{-2} was used to determine, and compensate for, losses due to ohmic resistance. 85% iR corrections were performed when measuring the kinetic overpotential of the electrocatalysts, and were critical when large-area FTO-coated glass substrates were used in the optical transmittance measurements.

For electrochemical measurements in 1.0 M KOH(aq), including photoelectrochemical measurements, spectral response behavior, and electrochemical impedance spectroscopy, a mercury/mercury oxide (Hg/HgO in 1.0 M KOH(aq), CH instruments, CH152) reference electrode was used, and a carbon cloth in a fritted glass tube (gas dispersion tube Pro-D, Aceglass, Inc.) was used as the counter electrode. The Hg/HgO reference electrode had a potential of 0.926 V versus the reversible hydrogen electrode, RHE.

For electrochemical measurements in 1.0 M H_2SO_4(aq) or 1.0 M K-Bi(aq), a SCE was used as the reference electrode and a fritted Pt mesh (0.5 mm diameter, 99.99% trace metal basis, Alfa, Aesar) was used as the counter electrode. For HER catalysts, the solutions were purged with high purity H_2(g) for 30 min prior to measurements of electrocatalytic activity for the HER, and the H_2(g) flow was maintained during such measurements. For measurements of electrocatalytic activity for the OER, solutions were pre-saturated using high purity O_2(g), and the O_2(g) flow was maintained during such measurements.

For Ni-based OER catalysts, 10 CVs were performed in the range 0.7 – 1.91 V versus RHE to activate the catalyst prior to characterization.

E. In situ Measurements of Optical Transmittance

In situ measurements of the optical transmittance of OER-catalyst-coated FTO-glass substrates were performed using a custom Teflon cell. Monochromatic light was incident upon a quartz window at an angle normal to the surface, as well as upon a calibrated Si photodiode (Thorlab Fs-100cal) that was isolated from the corrosive electrolyte by another quartz window. Samples were placed between the two quartz windows with the counter and reference electrodes out of the optical path. The exposed area of the Si photodiode was 0.03 cm^{-2}. The exposed areas of the sample electrodes (0.3-0.4 cm^{-2}) and the spot size of the incident light were both larger than the exposed area of the Si photodiode. The electrochromism of the sample was determined by monitoring the transmittance at a fixed illumination wavelength (550 nm) while scanning the applied potential in the range of 0.0–1.0 V versus Hg/HgO, or while galvanostatically holding the current density at 10 mA cm^{-2}. A peristaltic pump was used to circulate the electrolyte at a high circulation rate over the sample surface, to minimize the accumulation of bubbles and thus to minimize scattering of light by bubbles formed on the electrode surface. The transmittance was defined by the ratio between the transmission of catalyst-coated FTO substrates and the transmission of the bare FTO substrate.

HER catalysts are typically metallic and do not exhibit electrochromism under reductive conditions, so the optical transmittances of the HER catalysts were measured ex situ without applied cathodic bias.

The total optical transmittance was calculated using equation (1):

$$J = \frac{\int_{\lambda=350}^{1100} {}^{q}/_{hc} T(\lambda) \cdot P(\lambda) \cdot \lambda \cdot d\lambda}{\int_{\lambda=350}^{1100} {}^{q}/_{hc} P(\lambda) \cdot \lambda \cdot d\lambda} \quad (1)$$

where h is Planck's constant (6.63×10^{-34} J s), c is the speed of light (2.998×10^{8} m s^{-1}), q is unsigned elementary charge (1.602×10^{-19} C), T is the transmittance at each wavelength, P is the irradiance in W m^{-2} nm^{-1}, and λ is the light wavelength in nm. Figure S1 shows the in situ transmittance-measurement setup.

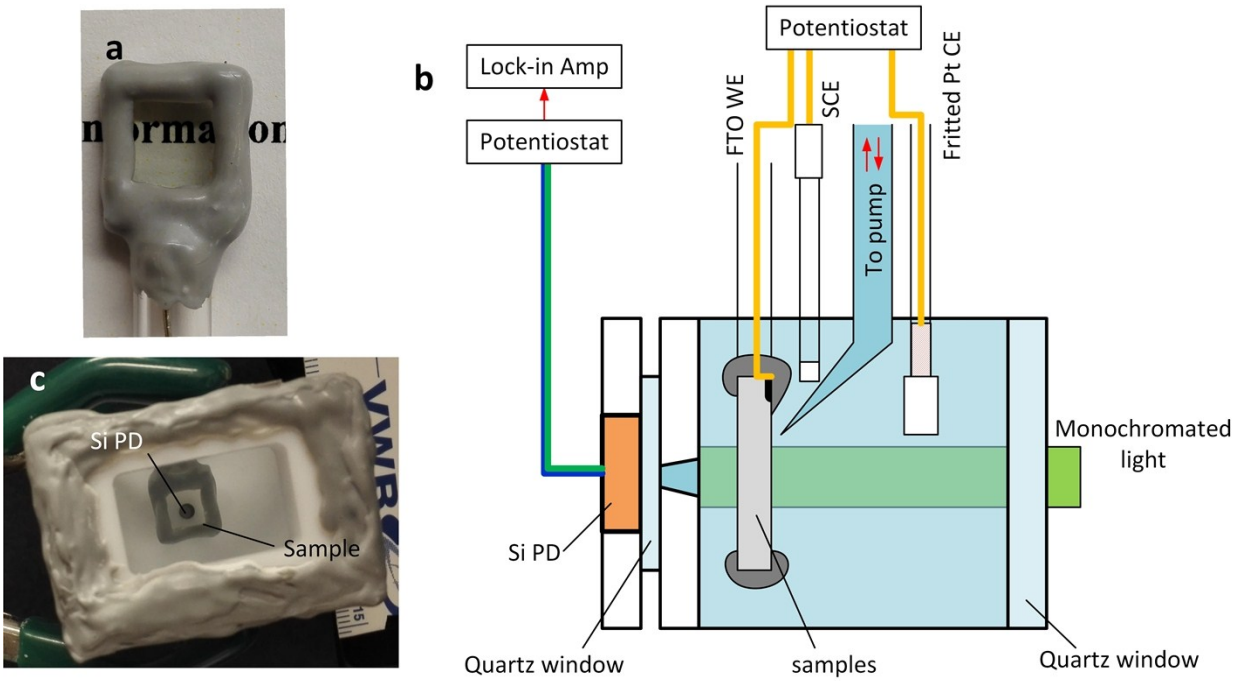

Figure S1. a) An optical image of a typical electrode for in situ optical transmittance measurements. b) A schematic of the experimental setup for the in situ optical transmittance measurements. Measurements were conducted at a constant current density of |10 mA cm^{-2}| with anodic current for OER catalysts and cathodic current for HER catalysts. Circulation was used to remove bubbles from electrode surface. A calibrated Si photodiode was used to measure the optical attenuation by the sample under working conditions. c) an optical image of an electrode in the measurement cell showing also the Si photodiode at the back. Other components are not shown in the image.

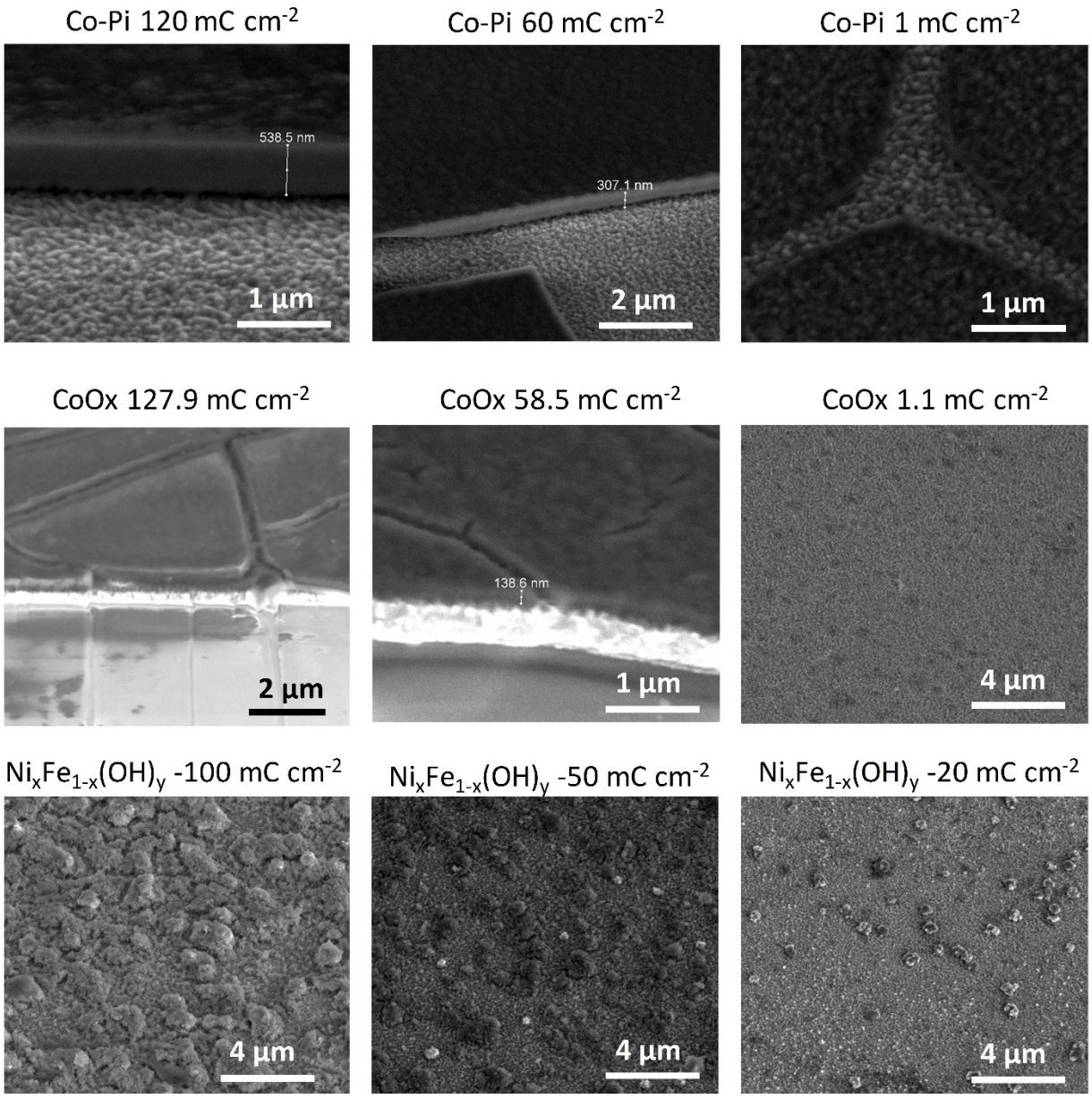

Figure S2. SEM images of electrocatalysts studied in this work including Co-Pi, CoO_x and $Ni_xFe_{1-x}(OH)_y$ at different loadings.

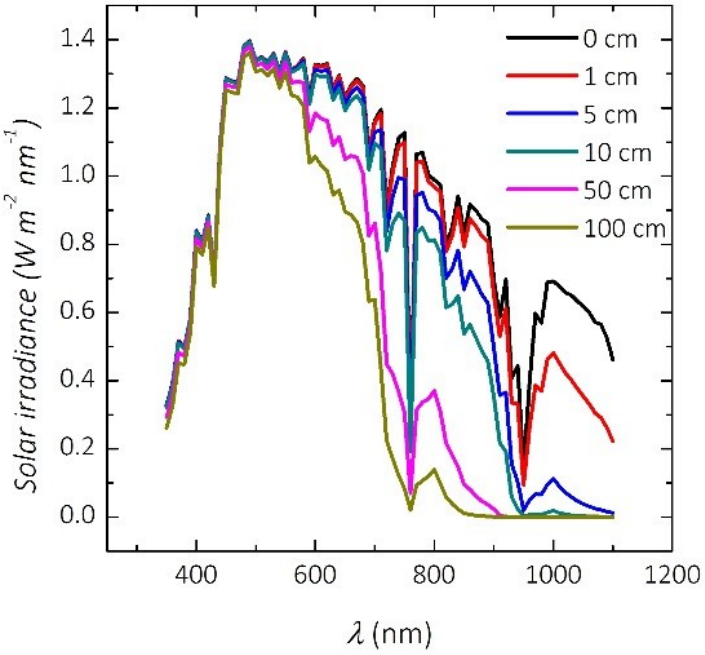

Figure S3. Solar irradiance spectra filtered by a water layer with different thicknesses showing increasing long-wavelength losses with increasing water-layer thickness.

The active surface areas of $CoO_{x,ed}$ were determined using the cathodic charge density (Q_c) measured in the pseudocapacitive region (Figure S3), which increased from 0.12 ± 0.02 mC cm^{-2}, to 0.58 ± 0.06, 10.06 ± 0.06 and 23.06 ± 1.48 mC cm^{-2}. A 20-fold increase in the active surface area thus reduced $\eta_{10\ mA\ cm\text{-}2}$ by ~67 mV.

As Q_d for the Co-Pi films was increased from 10 mC cm^{-2} to 60 or 120 mC cm^{-2}, respectively, Q_c increased from 1.18 ± 0.04 mC cm^{-2} to 2.46 ± 0.26 and 4.15 ± 0.16 mC cm^{-2}, respectively. The ratio between Q_c and Q_d is a measure of the deposition efficiency. This efficiency remained small (~0.03) and constant as Q_d increased for Co-Pi films. In contrast, for the $CoO_{x,ed}$ films, Q_d continuously increased from 0.10 to 0.18 during deposition. As the number

of ALD cycles increased from 60 (~3 nm) to 1000 cycles (~50 nm), Q_c (Figure 1c inset) remained constant at 0.082 ± 0.002 mC cm^{-2}. The distinctive redox peaks observed at ~1.1 V versus RHE (highlighted by red arrows in Figure S3 on $CoO_{x,ed}$ and Co-Pi films) were not observed for $CoO_{x,ALD}$ films in contact with 1.0 M KOH(aq).

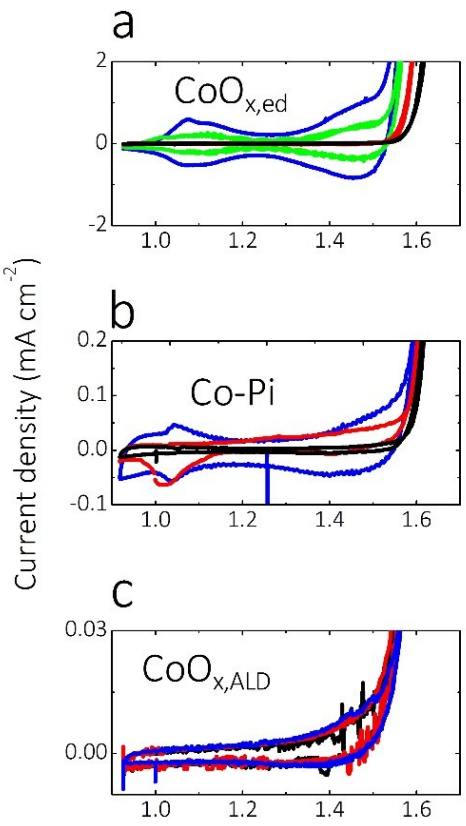

Figure S4. Dependence of redox peak area (Q_c) on method of preparation and material loading. a) $CoO_{x,ed}$, b) Co-Pi, and c) $CoO_{x,ALD}$.

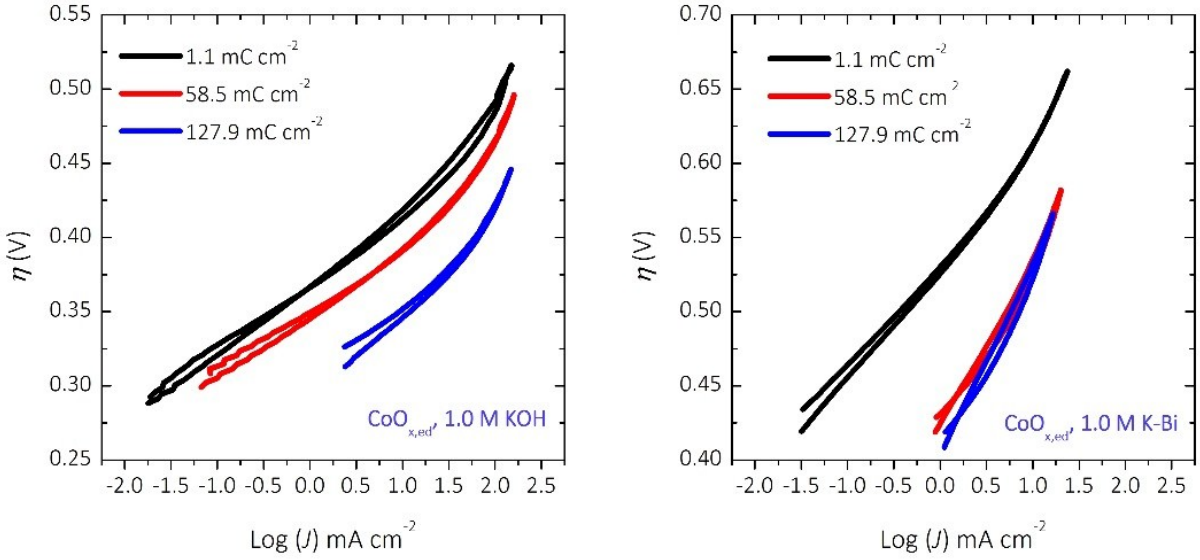

Figure S5. Tafel plots of $CoO_{x,ed}$ at different loadings in 1.0 M KOH(aq) and 1.0 M K-Bi(aq).

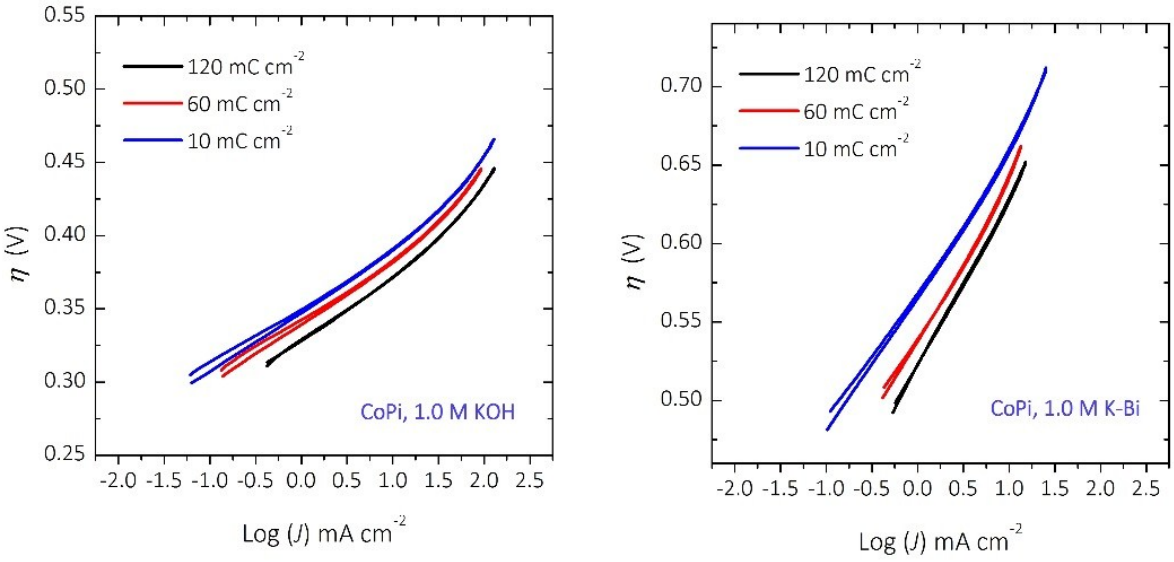

Figure S6. Tafel plots of Co-Pi at different loadings in 1.0 M KOH(aq) and 1.0 M K-Bi(aq).

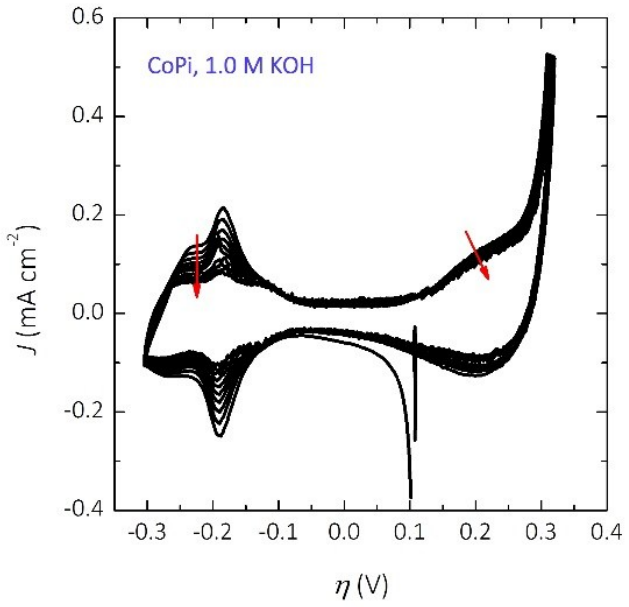

Figure S7. The *J-E* behavior showing a decrease of Q_c on Co-Pi at a loading of 120 mC cm^{-2} in 1.0 M KOH(aq) during 10 cycles of CV scans.

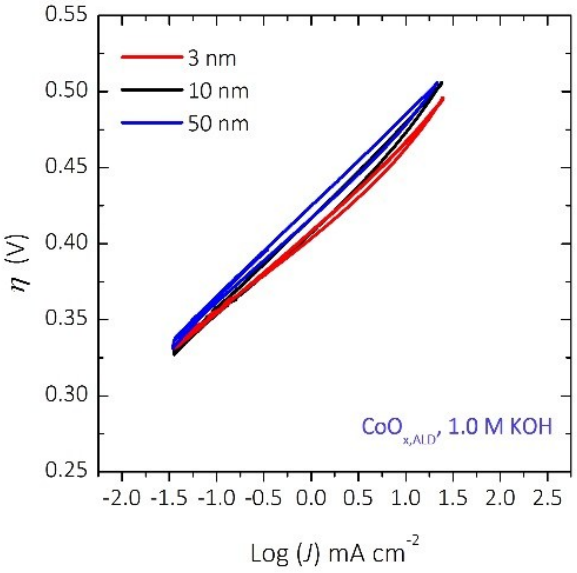

Figure S8. Tafel plot of $CoO_{x,ALD}$ at different loadings in 1.0 M KOH(aq).

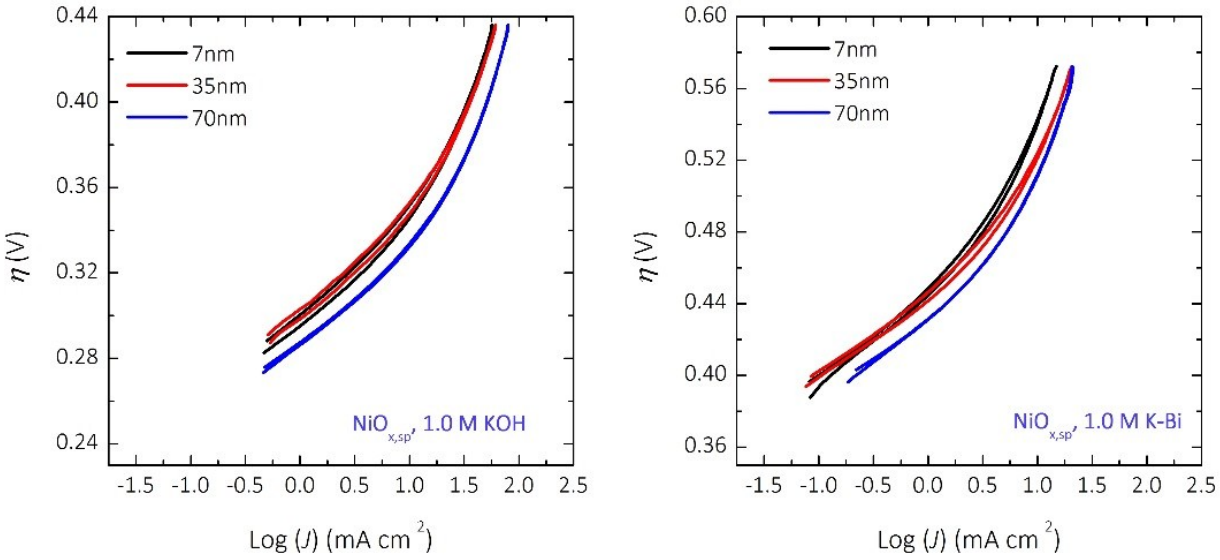

Figure S9. Tafel plots of $NiO_{x,sp}$ at different loadings in 1.0 M KOH(aq) and 1.0 M K-Bi(aq).

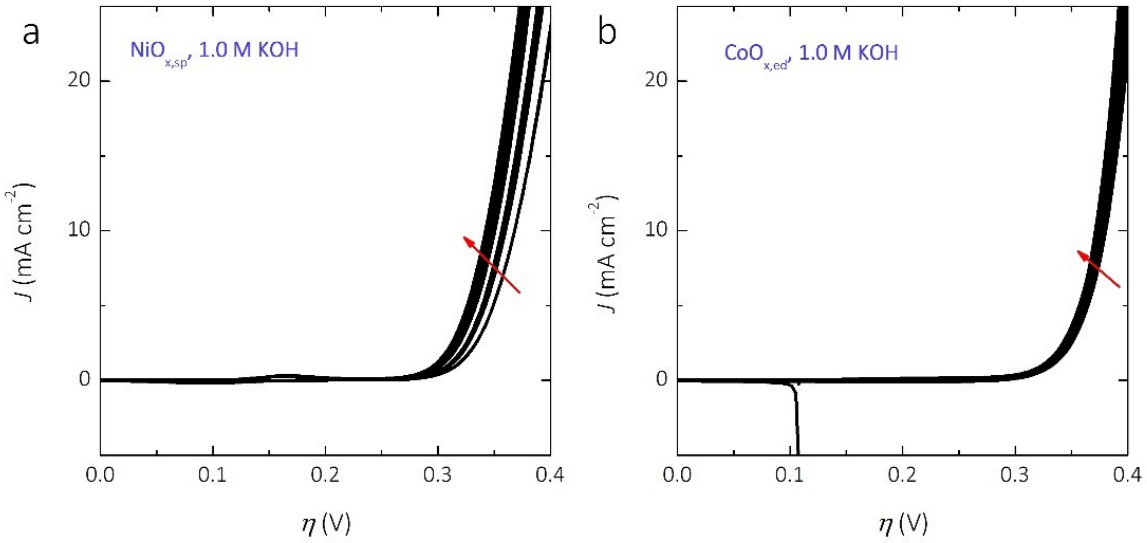

Figure S10. *J-E* behaviors of $NiO_{x,sp}$ at a loading of 70 nm (a) and $CoO_{x,ed}$ at a loading of 127.9 mC cm^{-2} (b) in 1.0 M KOH(aq) over 10 cycles of CV scans showing continuous improvement potentially caused by Fe contamination. Arrows in the figure indicate the direction of the shift of the *J-E* data over CV scans.

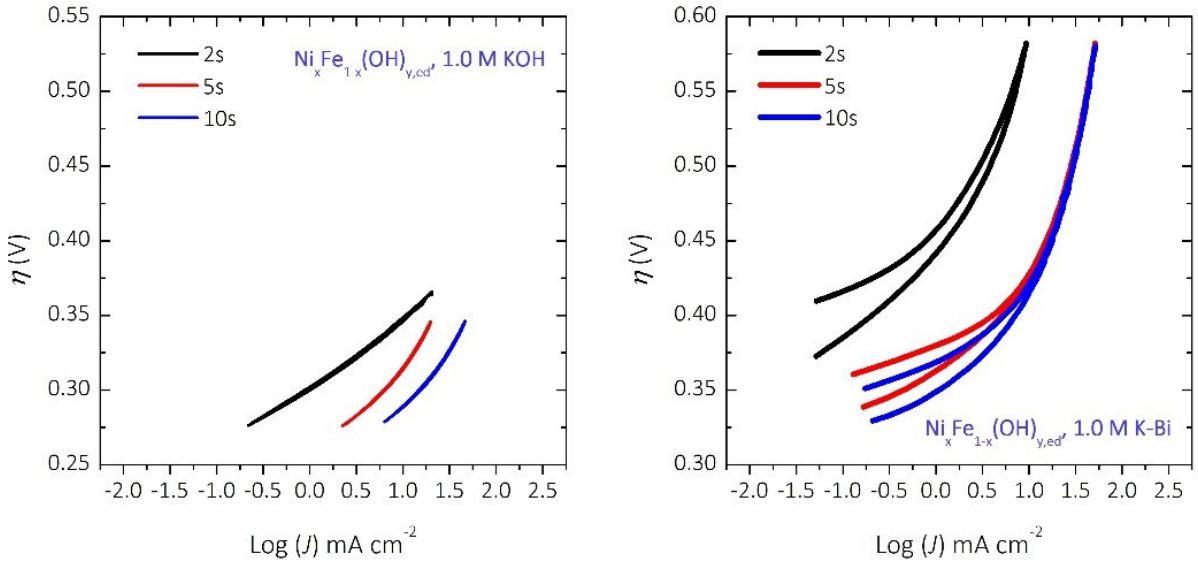

Figure S11. Tafel plots of $Ni_xFe_{1-x}(OH)_y$ at different loading in 1.0 M KOH(aq) and 1.0 M K-Bi(aq).

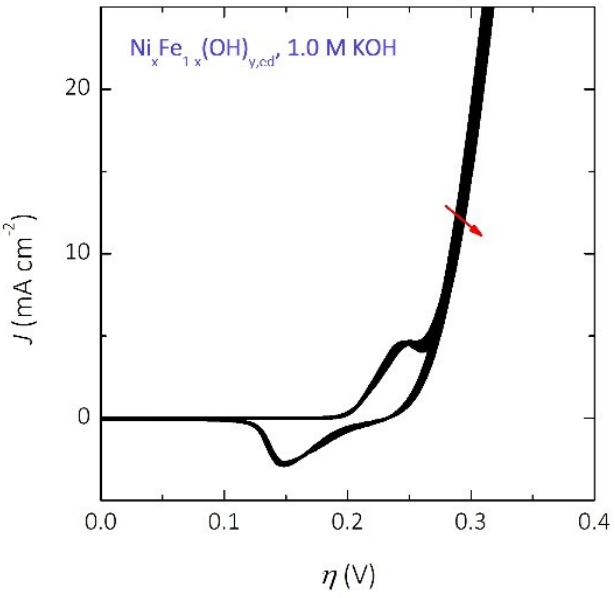

Figure S12. *J-E* behaviors of $Ni_xFe_{1-x}(OH)_{y,ed}$ at a loading of 10 s in 1.0 M KOH(aq) over 10 cycles of CV scans showing slight degradation. The arrow in the figure indicates the direction of the shift of the *J-E* data with additional CV scans.

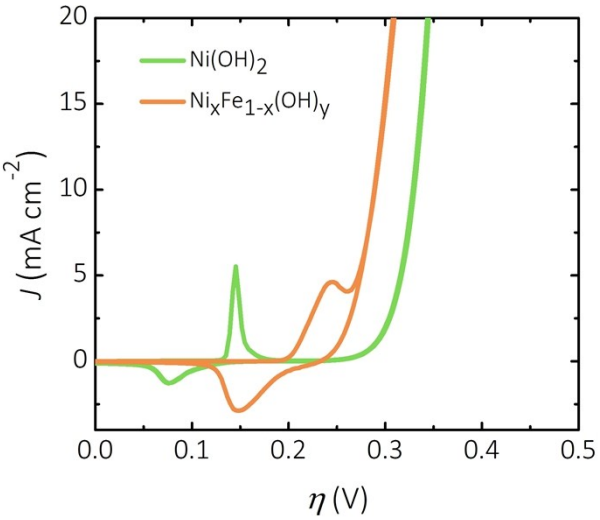

Figure S13. Comparison of polarization plots of $Ni(OH)_{2,ed}$ and $Ni_xFe_{1-x}(OH)_y$ at the highest loadings in 1.0 M KOH(aq).

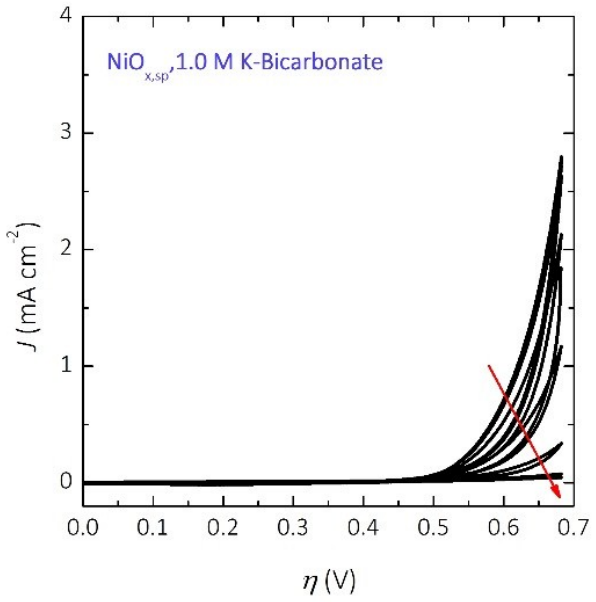

Figure S14. The *J-E* behavior showing a decrease of current density on $NiO_{x,sp}$ at a loading of 70 nm in 1.0 M K-bicarbonate(aq) during 10 cycles of CV scans. Arrow shows the shift of the *J-E* data over CV scans.

Ir and Ru based oxides are the only reported dimensionally stable and active catalysts for electrochemical water oxidation in acidic media, both of which are scarce and expensive. We also note that there are recent reported efforts directed toward the development of acid-stable OER catalysts based on earth-abundant elements. In fact, Ir and Ru by themselves have shown corrosion under operational conditions and poor kinetics. Some metal oxides (Ta, Sn, Ti, Si, Ce, Ni, Co, Nb, and etc) have been used together with Ir or Ru to form metal oxide alloys to improve the catalytic activity and electrochemical stability.

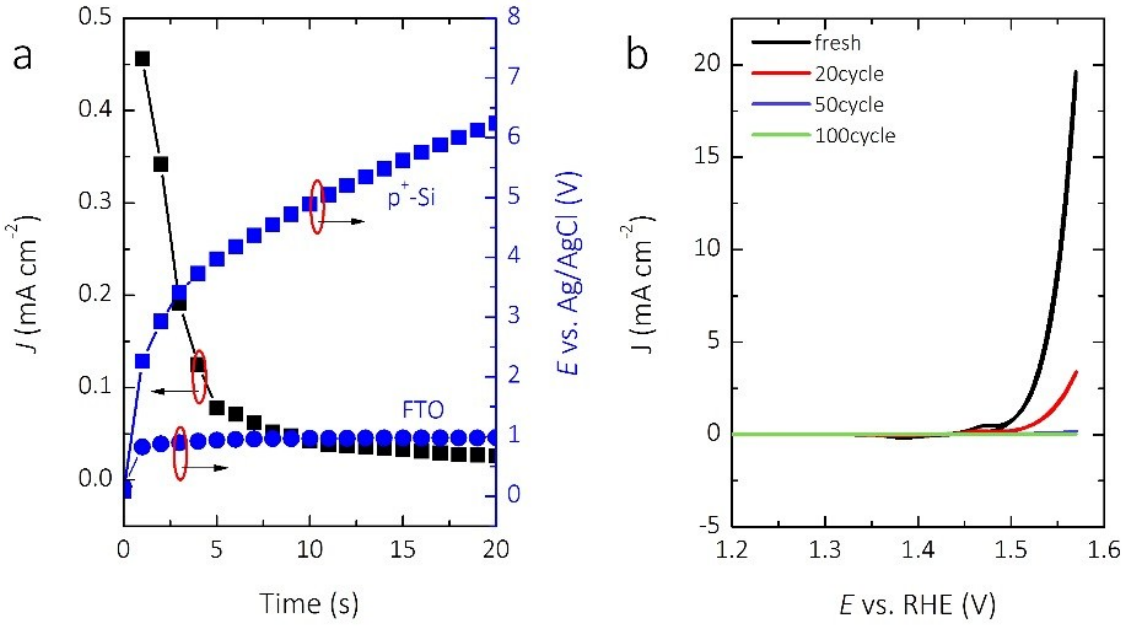

Figure S15. a) Representative chronoamperometric (black curve) and chronopotentiometric (blue curves) behaviors observed during deposition of Co-Pi on freshly HF-etched p^+-Si and FTO-glass substrates, and b) *J-E* behavior of $Ni_xFe_{1-x}(OH)_{y,ed}$ coated p^+-Si substrates showing degradation over 100 cycles of cyclic voltammetric scans.

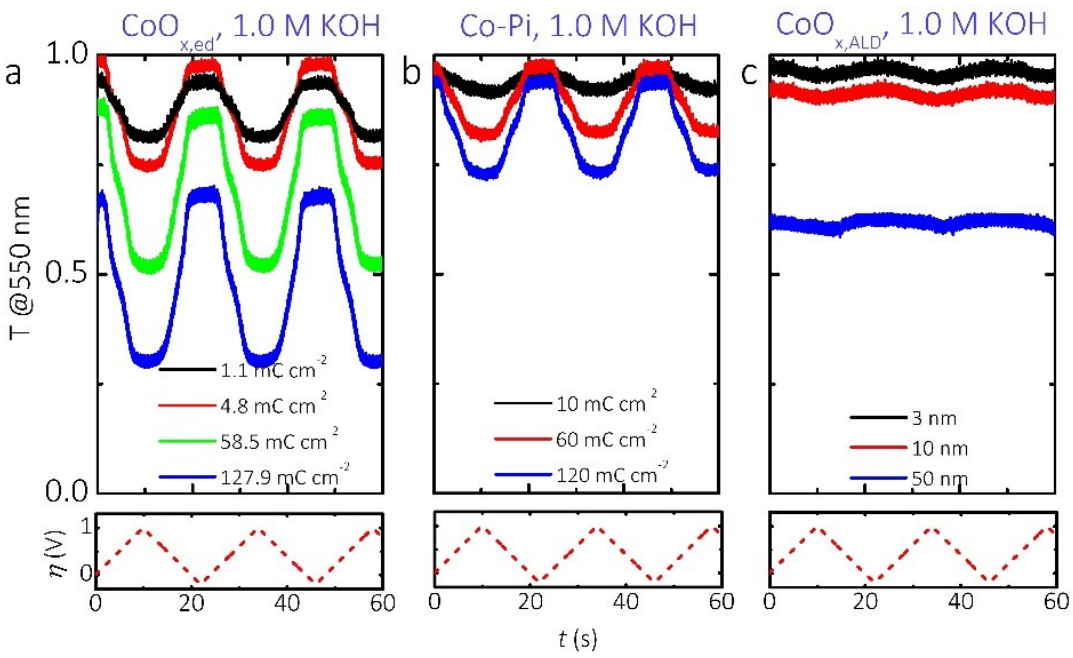

Figure S16. Potential-dependent dynamic transmittance at a fixed illumination wavelength of 550 nm on $CoO_{x,ed}$, Co-Pi, and $CoO_{x,ALD}$ at different loadings. a) $CoO_{x,ed}$ showed increased electrochromism and reduced transmittance at the bleached state with increasing catalyst loading. b) Co-Pi showed increased electrochromism, but negligible change in transmittance at the bleached state with increased catalyst loading. b) $CoO_{x,ALD}$ showed reduced transmittance at the bleached state and negligible electrochromism with increasing catalyst loading.

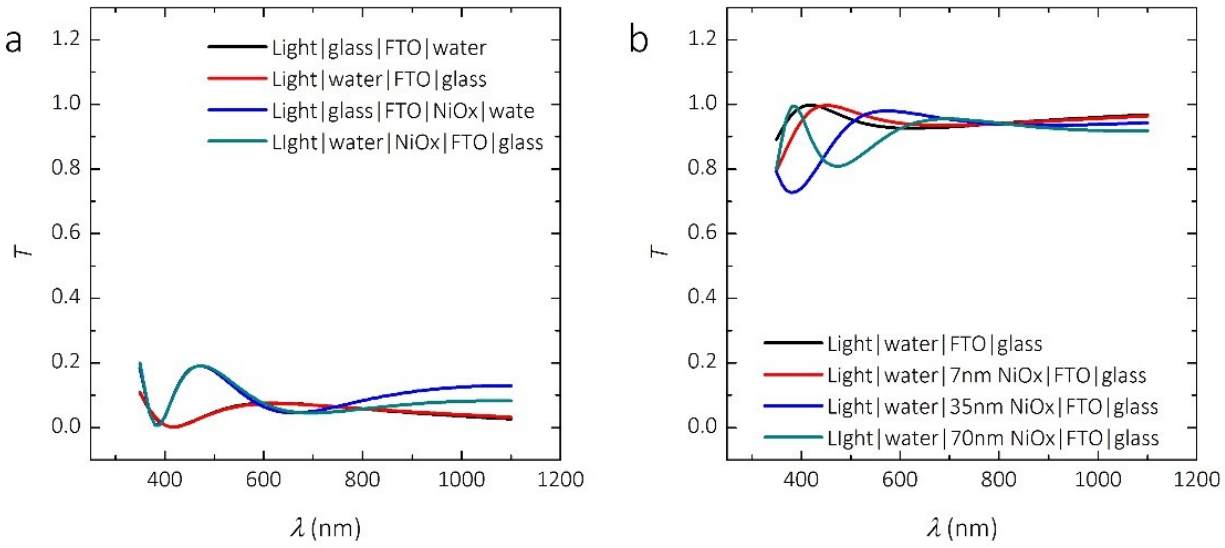

Figure S17. A) Reflectance spectra on FTO glass with and without a NiO_x coating showing negligible effects from the direction of the incident, and b) calculated NiO_x thickness-dependent transmittance spectra. The total reflectances of the samples versus wavelength, with different NiO_x thickness varied from 0-70 nm with water as incident media and illuminated under various incidence angles, were calculated based on the propagation matrix of plane waves at dielectric interfaces. The Matlab function (multidiel) developed by Sophocles J. Orfanidis from Rutgers University, was used to calculate the reflection responses of the isotropic non-lossy multilayer dielectric structures[3]. Optical constants for water, FTO, glass and NiO_x were adopted from peviously reported values[4].

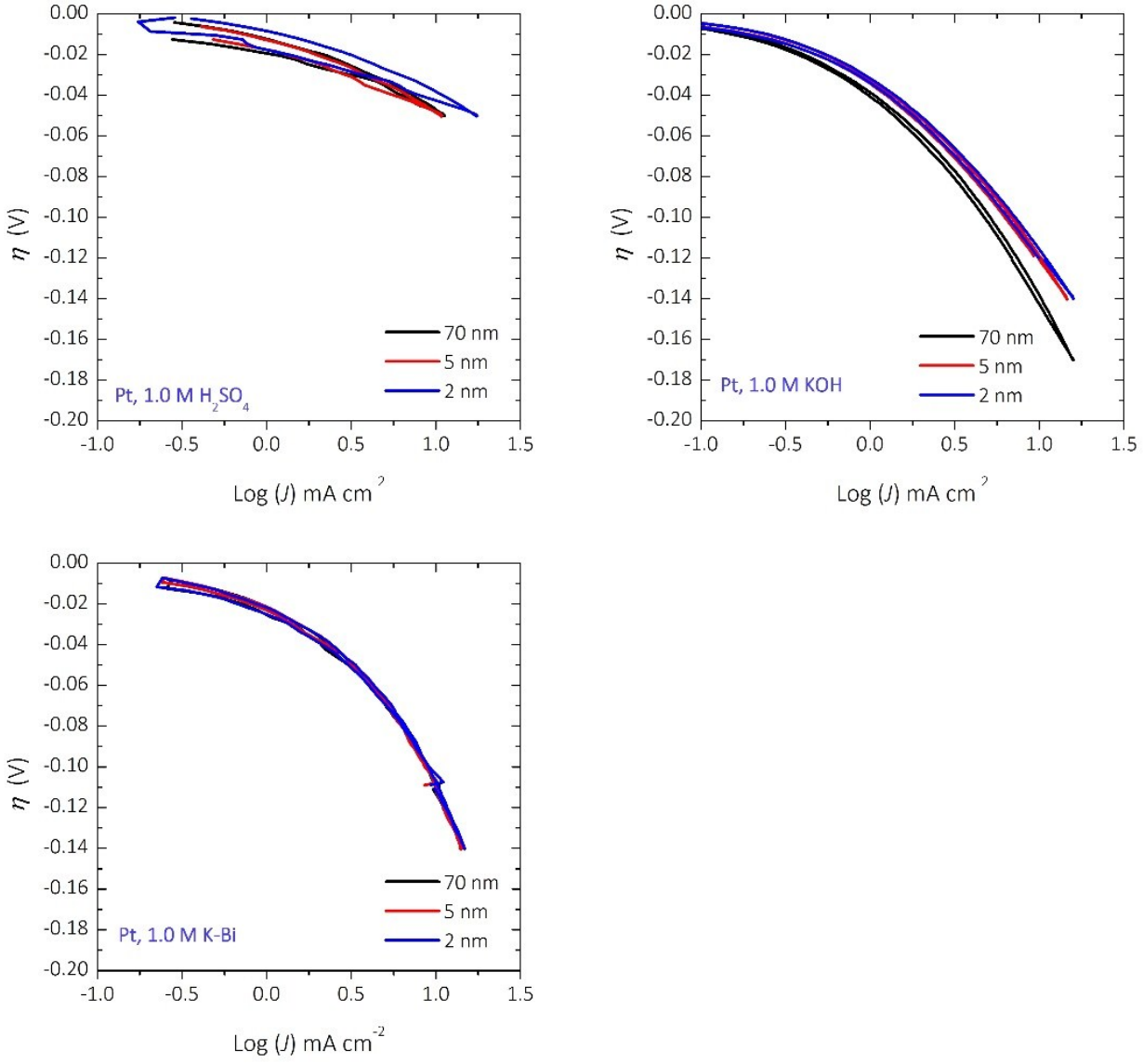

Figure S18. Tafel plots of sputtered Pt films in various electrolytes showing no loading effect within the thickness range studied.

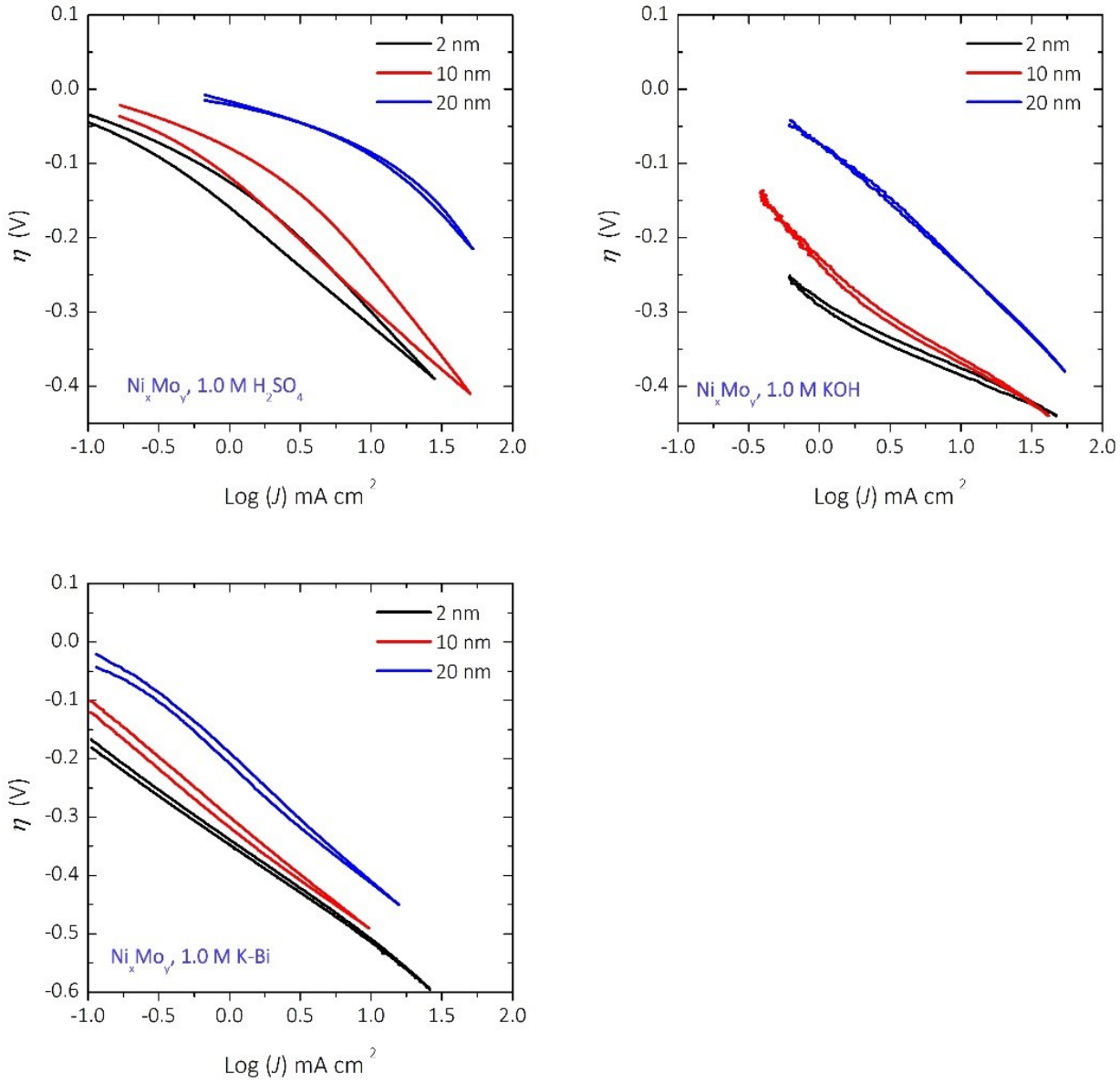

Figure S19. Tafel plots of sputtered Ni_xMo_y films showing the loading effect in various electrolytes.

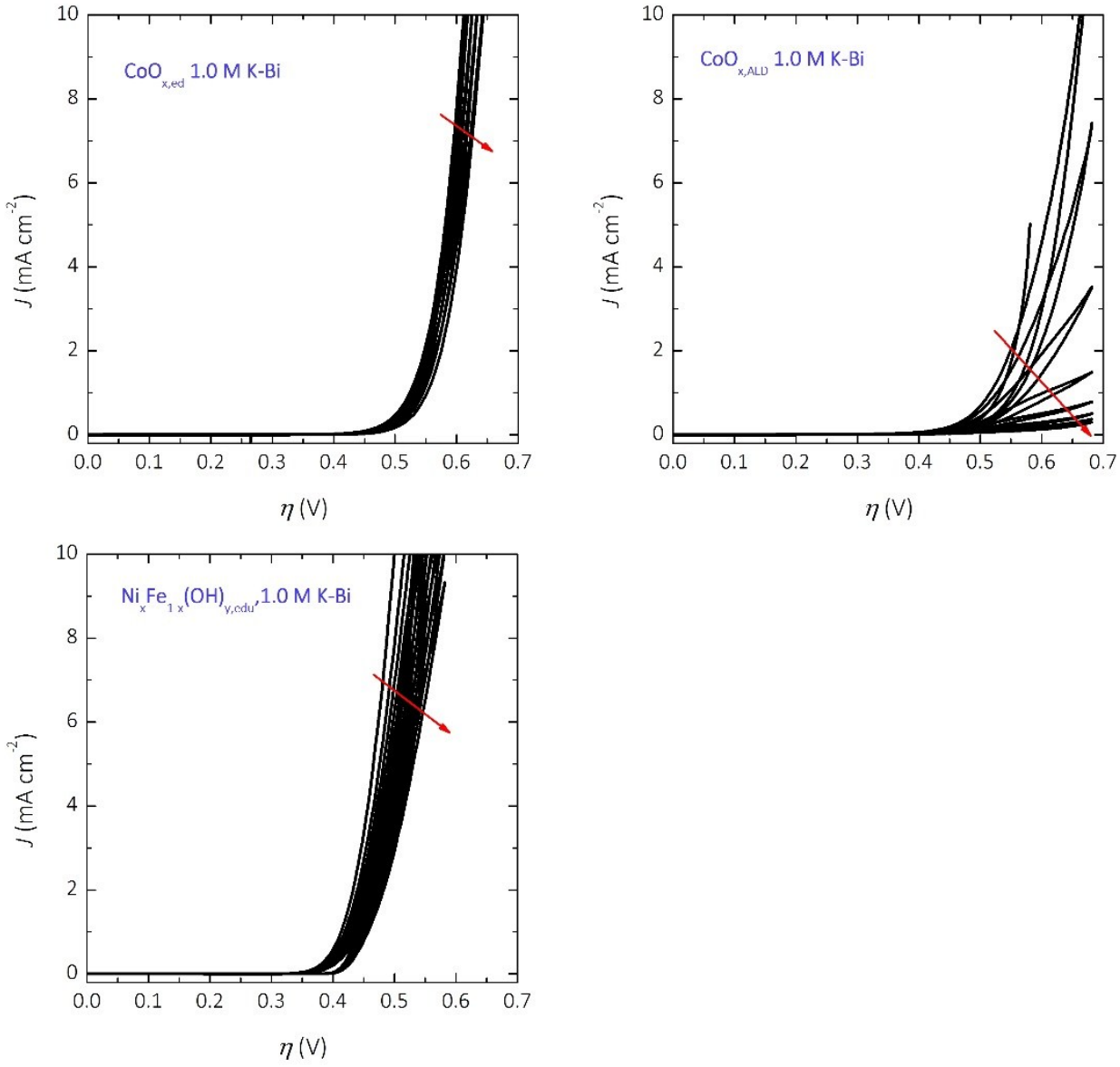

Figure S20. *J-E* behaviors of $CoO_{x,ed}$ at a loading of 127.9 mC cm^{-2} (a), $CoO_{x,ALD}$ at a loading of 50 nm (b), and $Ni_xFe_{1-x}(OH)_{y,ed}$ at a loading of 2 s (c) in 1.0 M K-Bi(aq) during 10 cycles of CV scans.

Supporting table:

Table S1. Efficiency and band-gap combinations for solar fuels devices based on a tandem light absorber with a photocathode top cell and Si photoanode bottom cell, in contact with 1.0 M H_2SO_4(aq) as a function of the loading of a Pt catalyst film. Efficiencies are calculated based on a tandem cell with a fixed band-gap combination of 1.70 eV/1.12 eV (entries above the double horizontal line), and based on tandem cells with the band gap for the photoanode optimized for the properties of the Pt catalyst film (entries below the double horizontal line). Ru was used as an OER catalyst in acidic condition with an overpotential loss of 350 mV.

Pt loading (nm)	Top junction (1.70 eV) current density (mA cm^{-2})	Bottom junction (1.12 eV) current density (mA cm^{-2})	Total overpotential loss ($\eta_{OER+HER}$/mV)	Integrated transmittance (%)	STH Efficiency (%)
2	18.6	14.3	397	83	17.6
5	10.6	7.2	398	45	10.6
70	<0.1	<0.1	390	<0.4	<0.1
Pt loading (nm)	Top junction band gap	Bottom junction band	Total overpotential	Integrated transmittance	Efficiency (%)

	(eV)	gap (eV)	loss ($\eta_{OER+HER}$/mV)	(%)	
2	1.80	1.12	397	83	20.2
5	1.85	1.12	398	45	11.0
70	1.85	1.12	390	<0.4	<0.1

Table S2. Efficiency and band-gap combinations for solar fuels devices based on a tandem light absorber with a photocathode top cell and Si photoanode bottom cell, in contact with 1.0 M KOH(aq) as a function of the loading of a NiMo catalyst film. Efficiencies are calculated based on a tandem cell with a fixed band-gap combination of 1.70 eV/1.12 eV (entries above the double horizontal line), and based on tandem cells with the band gap for the photoanode optimized for the properties of the Pt catalyst film (entries below the double horizontal line). NiFeOOH was used as an OER catalyst in alkaline condition with an overpotential loss of 280 mV.

NiMo loading (nm)	Top junction (1.70 eV) current density (mA cm^{-2})	Bottom junction (1.12 eV) current density (mA cm^{-2})	Total overpotential loss ($\eta_{OER+HER}$/mV)	Integrated transmittance (%)	STH Efficiency (%)
2	16.0	12.0	663	71	14.8

10	5.1	3.8	632	23	4.7
20	<0.1	<0.1	510	~0.4	<0.1
NiMo loading (nm)	Top junction band gap (eV)	Bottom junction band gap (eV)	Total overpotential loss ($\eta_{OER+HER}$/mV)	Integrated transmittance (%)	Efficiency (%)
2	1.80	1.12	663	71	17.1
10	1.81	1.12	632	23	5.5
20	1.65	1.12	510	~0.4	0.1

II. REFERENCES:

1. C. N. P. da Fonseca, M.-A. De Paoli and A. Gorenstein, *Adv. Mater.*, 1991, **3**, 553-555.
2. Y. Surendranath, M. W. Kanan and D. G. Nocera, *J. Am. Chem. Soc.*, 2010, **132**, 16501-16509.
3. S. J. Orfanidis, *Electromagnetic waves and antennas*, 2014.
4. K. Sun, F. H. Saadi, M. F. Lichterman, W. G. Hale, H.-P. Wang, X. Zhou, N. T. Plymale, S. T. Omelchenko, J.-H. He, K. M. Papadantonakis, B. S. Brunschwig and N. S. Lewis, *Proc. Natl. Acad. Sci. USA*, 2015, **112**, 3612-3617.